Electrocatalysts

International Edition: DOI: 10.1002/anie.201906394
German Edition: DOI: 10.1002/ange.201906394

Promoting Subordinate, Efficient Ruthenium Sites with Interstitial Silicon for Pt-Like Electrocatalytic Activity

*Hui Chen[+], Xuan Ai[+], Wang Liu, Zhoubing Xie, Weiqiang Feng, Wei Chen, and Xiaoxin Zou**

Abstract: *The fundamental understanding and rational manipulation of catalytic site preference at extended solid surfaces is crucial in the search for advanced catalysts. Herein we find that the Ru top sites at metallic ruthenium surface have efficient Pt-like activity for the hydrogen evolution reaction (HER), but they are subordinate to their adjacent, less active Ru_3-hollow sites due to the stronger hydrogen-binding ability of the latter. We also present an interstitial incorporation strategy for the promotion of the Ru top sites from subordinate to dominant character, while maintaining Pt-like catalytic activity. Our combined theoretical and experimental studies further identify intermetallic RuSi as a highly active, non-Pt material for catalyzing the HER, because of its suitable electronic structure governed by a good balance of ligand and strain effects.*

The in-depth understanding of characteristics of catalytic sites at extended solid surfaces is instructive for rational catalyst design. The Sabatier principle presents a general qualitative rule: for an optimal catalyst the bond between the catalytic site and the key intermediate should have moderate strength.[1] That is, a good catalyst should bind the key intermediate to its catalytic site strongly enough to activate it, yet not too strongly so that the product can desorb. Benefiting from the progress in density functional theory (DFT) calculations, researchers can use the adsorption energy of the reaction intermediate to quantitatively describe the bond strength and thereby evaluate the catalytic activity of each surface site.[2] At a complex, extended solid surface, there are usually several types of possible catalytic sites with different adsorption properties (also known as catalytic site diversity). The most stable adsorption sites are the most favorable ones for catalysis, and their activities more closely reflect the real activity of catalyst (also known as catalytic site dominance).[3] Thus, for a given catalytic site to be desirable, it should possess a moderate ability to bind the key intermediate, while simultaneously being dominant to other adjacent sites.

To demonstrate this idea, we chose hydrogen evolution reaction (HER) electrocatalysis as a model reaction, which is involved in many renewable energy-related technologies. The adsorption free energy of atomic hydrogen (ΔG_{H^*}) is proven to be a reliable descriptor for quantifying the aforementioned bond strength and thereby evaluating the HER activity of a given catalytic site.[4] For an optimum HER catalyst, its catalytic sites should have a near-zero ΔG_{H^*} value. The benchmark catalyst Pt is such a material with suitable hydrogen adsorption properties. While a number of inexpensive materials have been identified as promising alternatives to expensive Pt catalysts,[5] most of them still exhibit catalytic activity much lower than that of Pt. Very recently, despite the fact that metallic Ru shows an intrinsically moderate HER activity, a few Ru-based nanomaterials,[6] especially those coupled with nanocarbons, were found to give remarkable HER activity close to that of the Pt catalysts. However, it remains unclear what changes in the Ru-based catalytic sites are responsible for the activity enhancement, and a general guiding principle for engineering Ru-based catalytic sites is also not available.

Herein, we present a combined theoretical and experimental study that reveals the importance of catalytic site preference for the catalytic HER activity of Ru-based catalysts. We find that although the Ru top sites at the surface of metallic Ru have Pt-like catalytic activity for HER, they are subordinate to the adjacent, less active Ru_3-hollow sites. By incorporating appropriate interstitial atoms to form intermetallics, we can promote the subordinate, efficient Ru top sites, generating a novel non-Pt HER catalyst with Pt-like activity.

DFT calculations were conducted to evaluate the H adsorption properties and HER activities of the possible catalytic sites on the Ru(0001) surface (Figure S1 and Table S1 in the Supporting Information), a representative model surface of metallic Ru.[7] The results (Figure 1a) show that the stable H adsorption sites on the Ru(0001) surface include the Ru top site and two types of Ru_3-hollow sites (i.e., h1 and h2 sites). Figure 1b and Figure S2 further reveal that the Ru top site has a near-zero ΔG_{H^*} (−0.07 eV), whereas the Ru_3-hollow sites give largely negative ΔG_{H^*} values of around −0.45 eV. This indicates that despite its high Pt-like catalytic activity for HER, the Ru top site is subordinate because its rival sites, the adjacent Ru_3-hollow sites, are energetically more favorable for hydrogen adsorption.

In order to promote the catalytic activity of the highly active Ru top site from subordinate to dominant character, we present a strategy based on interstitial incorporation to

[*] Dr. H. Chen,[+] X. Ai,[+] W. Liu, Z. Xie, Prof. X. Zou
State Key Laboratory of Inorganic Synthesis and Preparative Chemistry, College of Chemistry
Jilin University, Changchun 130012 (China)
E-mail: xxzou@jlu.edu.cn
W. Feng
College of Materials Science and Engineering
Jilin University, Changchun 130012 (China)
Prof. W. Chen
Laboratory of Theoretical and Computational Chemistry
Institute of Theoretical Chemistry
Jilin University, Changchun 130023 (China)
[+] These authors contributed equally to this work.
Supporting information and the ORCID identification number(s) for the author(s) of this article can be found under: https://doi.org/10.1002/anie.201906394.

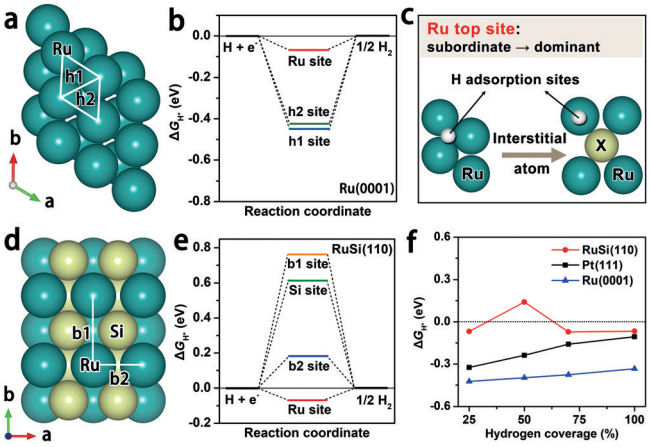

Figure 1. a) The stable H adsorption sites and b) their calculated ΔG_{H^*} values on the Ru(0001) surface. c) Schematic illustration of the interstitial incorporation strategy for transformation of Ru top sites from subordinate to dominant character. d) The stable H adsorption sites and e) their calculated ΔG_{H^*} values on the RuSi(110) surface. f) ΔG_{H^*} values at various hydrogen coverages for the h1 site on the Ru(0001) surface, the Ru top site on the RuSi(110) surface, and the Pt top site on the Pt(111) surface.

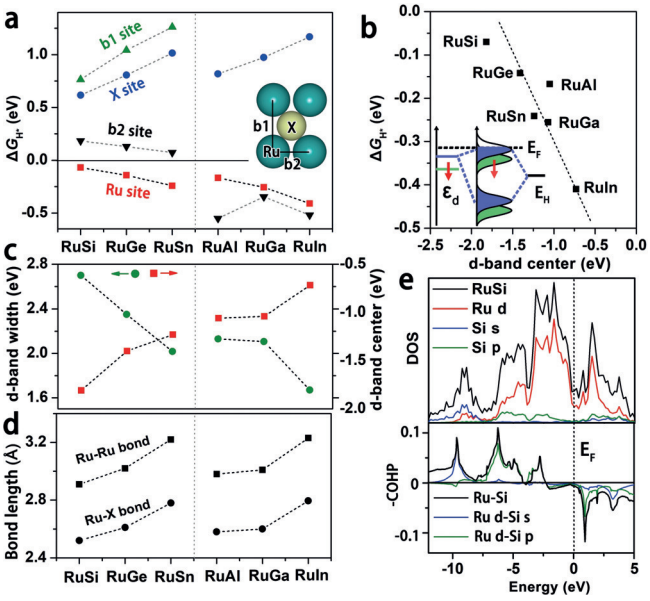

Figure 2. a) Calculated ΔG_{H^*} values at stable H adsorption sites on RuX(110) surfaces; the inset gives stable H adsorption sites on RuX(110) surfaces. b) Relationship between ΔG_{H^*} at the Ru top site and the Ru d-band center; the inset explains how the variation of the d-band center affects H adsorption energy. c) The d-band center and corresponding d-band width of the RuX(110) surfaces. d) The Ru–Ru and Ru–X bond lengths of the six RuX intermetallics. e) Calculated DOS of the RuSi(110) surface and COHP of the Ru–Si bond.

eliminate the Ru_3-hollow sites (Figure 1c). Silicon is found to be an appropriate interstitial atom through the construction of a CsCl-type RuSi intermetallic structure. The (110) surface of RuSi is the most exposed surface (Figure S3 and Table S2) and accounts for a surface proportion of 85% within the Wulff construction (Figure S4). Hence, the RuSi(110) surface was studied through further DFT calculations (Figure S5 and Table S3). As shown in Figure 1d, the Ru atoms are isolated from each other by the neighboring Si atoms and the Ru_3-hollow site disappears. The stable H adsorption sites on the RuSi(110) surface include two top sites (Ru and Si top sites) and two bridge sites (b1 and b2 sites). Among these catalytic sites (Figure 1e), the Ru top site on the RuSi(110) surface is found to be the most favorable (or dominant site) for hydrogen adsorption, whilst maintaining the near-zero ΔG_{H^*} or Pt-like catalytic activity.

Figure 1f presents a comparison of ΔG_{H^*} values at the preferred adsorption sites on RuSi(110), Ru(0001), and Pt(111) surfaces (the model surface of Pt) under different H* coverages (θ_{H^*}). The results show that the absolute values of ΔG_{H^*} for the RuSi(110) surface are close to zero over the entire θ_{H^*} range, and they are smaller than those for the Ru(0001) and Pt(111) surfaces. This result further suggests that RuSi should be a very competitive, non-Pt material for catalyzing the HER.

To further understand the role of Si interstitial atoms, a family of six CsCl-type RuX intermetallics (X = Si, Ge, Sn, Al, Ga and In) were investigated (Tables S3–S8). Figure 2a presents the stable H adsorption sites on the RuX(110) surfaces and their corresponding ΔG_{H^*} values. The results show that: 1) The RuX intermetallics (X = Si, Ge, and Sn) have energetically favorable adsorption at the Ru top site, with RuSi exhibiting the most optimal ΔG_{H^*} value; 2) The absolute ΔG_{H^*} values at the Ru top site periodically increase in the order: RuSi < RuGe < RuSn and RuAl < RuGa < RuIn. These results indicate that besides the local geometric structure of the Ru catalytic site, its electronic structure is also crucial for realizing efficient catalytic activity. Figure 2b,c shows a good linear correlation between ΔG_{H^*} at the Ru top site and the d-band center, and an inverse relationship between the d-band center and the d-band width, two key characteristics of the electronic structure (Figure S6 and Table S9). As the d-band center becomes more negative relative to the Fermi level (Figure 2b, inset), the antibonding states become more occupied, resulting in weaker H adsorption. Among the six RuX intermetallics, RuSi exhibits the most negative d-band center and near-zero ΔG_{H^*} at the Ru top site.

Next, we attribute the modification of electronic properties in RuX to a combination of strain and ligand effects.[8] On the one hand, the incorporation of interstitial atoms in Ru can generate chemical strain and thereby result in the expansion of the crystal lattice. All six RuX intermetallics have much longer Ru–Ru bonds than metallic Ru (2.73 Å), and the Ru–Ru bond lengths increase in the order: RuSi < RuGe < RuSn and RuAl < RuGa < RuIn (Figure 2d). This variation is similar to the trend in electronic structure (Figure 2c). This result implies that the tensile strain, which can decrease the metal d-orbital overlap and lead to a narrower band width and a more positive d-band center, is a significant factor responsible for the change of electronic properties. On the other hand, orbital hybridization between Ru and X atoms (termed the ligand effect) is another significant factor that can modify the electronic structure. The ligand effect always

results in a broadening of the metal d-band and a more negative d-band center.

The strongly negative d-band center of RuSi can be explained by the fact that among the six RuX intermetallics (Figure 2d and Table S10), for RuSi the smallest expansion in the Ru–Ru bond length results in the weakest strain effect, and simultaneously, the shortest Ru–X bond length means the strongest orbital hybridization between Ru and X atoms (or ligand effect). The orbital hybridization between Ru and Si atoms in RuSi was studied by its density of the states (DOS) and the crystal orbital Hamiltonian population (COHP) for the Ru−Si bond (Figure 2e). The results reveal that there is a DOS overlap and bonding between the Ru 3d orbital and the Si 2s-2p orbitals. Overall, the above results imply that the good balance of strain and ligand effects in RuSi lend it a suitable electronic structure and thus a near-zero ΔG_{H^*} value at the Ru top site.

Inspired by these theoretical results, we synthesized the RuSi material and then investigated its electrocatalytic activity for the HER. The standard synthesis of phase-pure RuSi is the direct reaction of ruthenium–silicon powders at high pressure (> 7.8 GPa).[9] Here, we present a synthesis of phase-pure RuSi nanoparticles without high pressure by employing a magnesiothermic reduction reaction with $RuCl_3$, Si, and Mg as the starting materials (see the Experimental Procedure in the Supporting Information). RuSi is formed under relatively mild conditions mainly because the new route has a significantly lower reaction enthalpy in comparison to that of the standard element reaction route (Figure S7). This method can also be extended to obtain the other ruthenium silicide phase, Ru_2Si_3 (Figures S8 and S9).

The X-ray diffraction (XRD) pattern of the as-synthesized sample confirms that the material contains single-phase RuSi (Figure 3a). The scanning electron microscopy (SEM) image (Figure 3b) reveals that the material is composed of RuSi nanoparticles 100–200 nm in size. Elemental mapping images (Figure 3c) show that the Ru and Si elements are homogeneously distributed over the entire nanoparticles. In the high-resolution transmission electron microscopy (HRTEM) image (Figure 3d), the interplanar distances of 0.29 nm and 0.21 nm can be assigned to the (001) and $(1\bar{1}0)$ crystallographic planes of RuSi, respectively. The angle of 90° between the two planes is consistent with the theoretical value. This result, coupled with the corresponding fast Fourier transform image (Figure 3d, inset), suggests that the exposed facet is {110}.

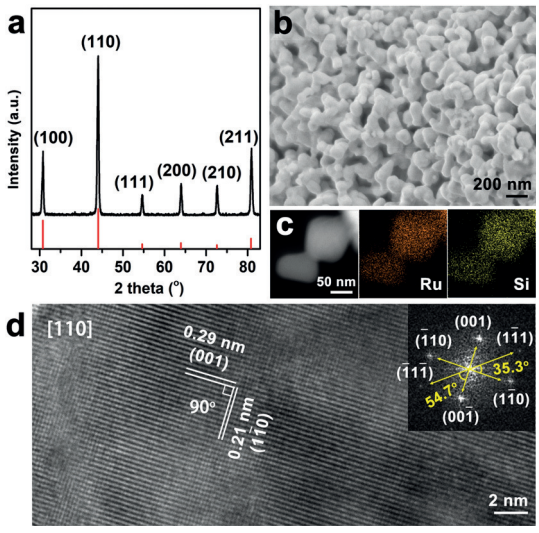

Figure 3. a) XRD pattern, b) SEM image, c) STEM image and the corresponding elemental mapping images, and d) HRTEM image of RuSi. Inset in (d) shows the corresponding fast Fourier transform image. The standard diffraction pattern for RuSi (red line) is also included in Figure 3a.

The RuSi material was further characterized by X-ray photoelectron spectroscopy (XPS) and X-ray absorption spectroscopy (XAS). XPS analysis indicates that the surface atomic ratio of Ru and Si is close to 1:1. Figure 4a shows

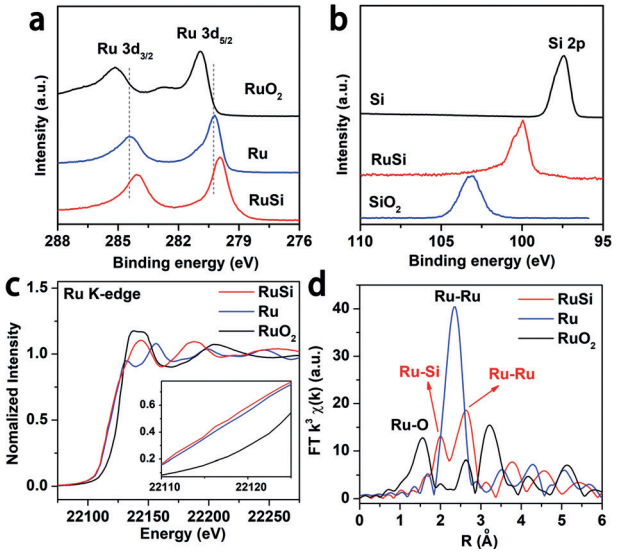

Figure 4. a) Ru 3d XPS spectra of RuSi, RuO_2, and Ru. b) Si 2p XPS spectra of RuSi, SiO_2, and Si. c) XANES spectra at the Ru K-edge of RuSi, RuO_2, and Ru; inset is an enlarged detail of (c). d) Fourier transforms of the EXAFS spectra of RuSi, RuO_2, and Ru. Note that the Fourier transforms are not corrected for phase shift, so that the peak positions in (d) are shorter than the actual bond lengths.

Ru 3d XPS spectra for RuSi and the reference samples (RuO_2 and Ru), and Figure 4b shows Si 2p XPS spectra for RuSi and the reference samples (SiO_2 and Si). The Ru 3d XPS peaks for RuSi exhibit a shift toward lower binding energy relative to that of metallic Ru, while the Si 2p XPS peak of RuSi shows a significant shift toward higher binding energy relative to that of Si. These results demonstrate that Ru atoms are negatively charged and Si atoms are positively charged in RuSi. The electron-richness of Ru atom in RuSi is also confirmed by X-ray absorption near-edge structure (XANES) spectra of the Ru K-edge, which shows that the energy of absorption edge of RuSi is slightly lower than that of metallic Ru (Figure 4c). The charge states of Ru and Si in RuSi are also examined by Bader charge analysis, which reveals that 0.8 electrons (| e |) transfer from the Si atom to the Ru atom. Although the charges on the Ru atom in RuSi and metallic Ru

are different, the transferred charges from the Ru atom to the adsorbed H atom are almost the same (Figure S10).

Figure 4d shows a comparison of the Fourier transforms of the extended X-ray absorption fine structure (EXAFS) at the Ru K-edge of three Ru-containing samples. There are two prominent peaks for RuSi, which correspond to the Ru–Si bond and the Ru–Ru bond. The Ru–Ru distance is longer than the Ru–Si distance in RuSi, and it is also longer than the Ru–Ru distance in metallic Ru. These results are consistent with crystallographic data (Table S10).

Next, the electrocatalytic activity of RuSi toward HER in acidic solution was studied (see the Experimental Section and Figure S11 in the Supporting Information). For comparative purposes, metallic Ru and Pt nanoparticles (Figures S12 and 13) were also synthesized and their catalytic activities were evaluated under the same conditions. Figure 5a shows the

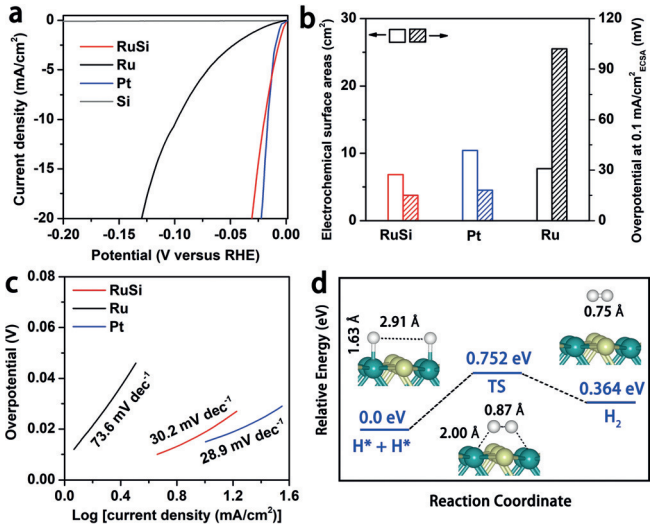

Figure 5. a) Polarization curves of RuSi, Ru, Pt, and Si in 0.5 M H_2SO_4 solution with 85% *iR* compensations. The current density is normalized by the geometric area of electrode. b) Comparison of ECSAs and overpotentials required at a current density of 0.1 mA cm^{-2} (normalized by ECSAs) in 0.5 M H_2SO_4 solution. c) Tafel plots for HER over RuSi, Ru, and Pt. d) Free energy diagrams of Tafel step of HER on the RuSi(110) surface; inset shows the optimized adsorption structures for the initial state, the transition state (TS), and the final state.

polarization curves for the HER over RuSi, Ru, Pt, and Si. While Si is inactive for HER, metallic Ru has a moderate catalytic activity. In contrast to Si and Ru, RuSi exhibits a remarkable catalytic activity toward HER, which is comparable to that of Pt and much better than that of Ru. In particular, RuSi requires an overpotential of 19 mV at 10 mA cm$_{geo}^{-2}$ current density (normalized by geometric area of the electrode). It is worth noting that the catalytic activity of RuSi is also similar to that of commercial 20 wt% Pt/C catalyst (Figure S14). In addition to high activity, RuSi displays good catalytic and structural stability during the HER (Figures S15 and S16). Moreover, RuSi gives nearly 100% faradaic efficiency during the HER (Figure S17), suggesting that the observed current can be attributed exclusively to the HER during electrocatalysis.

The specific activities of RuSi, Ru, and Pt were further compared by normalizing the measured currents with respect to electrochemical surface areas (ECSAs). Figure 5b shows the comparison of the ECSAs of the three materials and their specific activities, evaluated by the overpotential required at a current density of 0.1 mA cm$_{ECSA}^{-2}$. This comparison reveals that their specific activities follow almost the same trend as their geometric area normalized activities. The above results overall demonstrate that RuSi is a highly active, non-Pt material with Pt-like electroactivity for the HER.

Figure 5c shows the Tafel plots for RuSi, Ru, and Pt. RuSi displays a small Tafel slope of 28.9 mV dec^{-1}, which is comparable to that of Pt (30.2 mV dec^{-1}) and much smaller than that of Ru (73.6 mV dec^{-1}). This is in line with the rapid HER catalytic kinetics in the presence of RuSi. Additionally, the Tafel slope for RuSi suggests that hydrogen evolution over this material should occur via a Volmer–Tafel mechanism, in which the recombination of two adsorbed H atoms (H* + H* → H_2) is the rate-determining step.[10] Such a Volmer–Tafel mechanism on the RuSi(110) surface was also studied theoretically. Figure 5d presents three typical steps: 1) Two H atoms preferentially adsorb on adjacent Ru top sites with an H–H distance of 2.91 Å. 2) The two H atoms form a transition state (TS) with an H–H distance of 0.87 Å. 3) A H_2 molecule forms and desorbs from the RuSi surface. The calculated activation energy (0.75 eV) for the Tafel reaction on the RuSi(110) surface is a little lower than that on the Pt(111) surface (0.85 eV).[11] This result further suggests that RuSi is an efficient catalyst for HER.

In conclusion, we have demonstrated the importance of the manipulation of catalytic site preference for the rational design of advanced catalysts, with Ru-based HER electrocatalysts as model systems. We have also demonstrated that RuSi efficiently catalyzes the HER with Pt-like activity, due to the exposure of highly active Ru top sites.

Acknowledgements

X.Z. acknowledges financial support from National Key R&D Program of China (Grant No. 2017YFA0207800), the National Natural Science Foundation of China (NSFC) (Grant No. 21771079), Jilin Province Science and Technology Development Plan (20170101141JC), Program for JLU Science and Technology Innovative Research Team (JLUSTIRT), and Fok Ying Tung Education Foundation (Grant No. 161011). H.C. acknowledges financial support from the Postdoctoral Innovative Talent Support Program (Grant No. BX20180120) and the China Postdoctoral Science Foundation (Grant No. 2018M641771). W.C. acknowledges financial support from NSFC (21673093), Science and Technology Research Program of Education Department of Jilin Province (JJKH20190121KJ), and Jilin Province Science and Technology Development Plan (20170101175JC). We thank NSFC (21621001) and the 111 Project (B17020) for financial support. We thank the beamline BL14W (Shanghai Synchrotron Radiation Facility) for the XAS measurements.

Conflict of interest

The authors declare no conflict of interest.

Keywords: electrocatalysis · electronic structure · hydrogen evolution reaction · site preference

How to cite: *Angew. Chem. Int. Ed.* **2019**, *58*, 11409–11413
Angew. Chem. **2019**, *131*, 11531–11535

[1] a) M. Che, *Catal. Today* **2013**, *218–219*, 162–171; b) A. J. Medford, A. Vojvodic, J. S. Hummelshøj, J. Voss, F. A. Pedersen, F. Studt, T. Bligaard, A. Nilsson, J. K. Nørskov, *J. Catal.* **2015**, *328*, 36–42.

[2] a) Z. W. Seh, J. Kibsgaard, C. F. Dickens, I. Chorkendorff, J. K. Nørskov, T. F. Jaramillo, *Science* **2017**, *355*, eaad4998; b) Y. Zheng, Y. Jiao, M. Jaroniec, S. Z. Qiao, *Angew. Chem. Int. Ed.* **2015**, *54*, 52–65; *Angew. Chem.* **2015**, *127*, 52–66.

[3] a) W. Sheng, M. Myint, J. G. Chen, Y. Yan, *Energy Environ. Sci.* **2013**, *6*, 1509–1512; b) A. Plauck, E. E. Stangland, J. A. Dumesic, M. Mavrikakis, *Proc. Natl. Acad. Sci. USA* **2016**, *113*, E1973.

[4] B. Hinnemann, P. G. Moses, J. Bonde, K. P. Jørgensen, J. H. Nielsen, S. Horch, I. Chorkendorff, J. K. Nørskov, *J. Am. Chem. Soc.* **2005**, *127*, 5308–5309.

[5] For example: a) X. Zou, Y. Zhang, *Chem. Soc. Rev.* **2015**, *44*, 5148–5180; b) W. Wu, C. Niu, C. Wei, Y. Jia, C. Li, Q. Xu, *Angew. Chem. Int. Ed.* **2019**, *58*, 2029–2033; *Angew. Chem.* **2019**, *131*, 2051–2055; c) N. Han, K. R. Yang, Z. Lu, Y. Li, W. Xu, T. Gao, Z. Cai, Y. Zhang, V. S. Batista, W. Liu, X. Sun, *Nat. Commun.* **2018**, *9*, 924; d) I. S. Amiinu, Z. Pu, X. Liu, K. A. Owusu, H. G. R. Monestel, F. O. Boakye, H. Zhang, S. Mu, *Adv. Funct. Mater.* **2017**, *27*, 1702300.

[6] a) J. Mahmood, F. Li, S. M. Jung, M. S. Okyay, I. Ahmad, S. J. Kim, N. Park, H. Y. Jeong, J. B. Baek, *Nat. Nanotechnol.* **2017**, *12*, 441–446; b) Z.-L. Wang, K. Sun, J. Henzie, X. Hao, C. Li, T. Takei, Y.-M. Kang, Y. Yamauchi, *Angew. Chem. Int. Ed.* **2018**, *57*, 5848–5852; *Angew. Chem.* **2018**, *130*, 5950–5954; c) J. Wang, Z. Wei, S. Mao, H. Li, Y. Wang, *Energy Environ. Sci.* **2018**, *11*, 800–806; d) F. Li, G.-F. Han, H.-J. Noh, I. Ahmad, I.-Y. Jeon, J.-B. Baek, *Adv. Mater.* **2018**, *30*, 1803676.

[7] a) P. J. Feibelman, *Science* **2002**, *295*, 99; b) M. Pachecka, J. M. Sturm, C. J. Lee, F. Bijkerk, *J. Phys. Chem. C* **2017**, *121*, 6729.

[8] a) J. R. Kitchin, J. K. Nørskov, M. A. Barteau, J. G. Chen, *Phys. Rev. Lett.* **2004**, *93*, 156801; b) J. R. Kitchin, J. K. Nørskov, M. A. Barteau, J. G. Chen, *J. Chem. Phys.* **2004**, *120*, 10240; c) T. Adit Maark, A. A. Peterson, *J. Phys. Chem. C* **2014**, *118*, 4275.

[9] X. Lia, L. Xua, X. Cao, C. Meng, C. Wang, W. Zhu, *High Pressure Res.* **2013**, *33*, 8–14.

[10] D. Strmcnik, P. P. Lopes, B. Genorio, V. R. Stamenkovic, N. M. Markovic, *Nano Energy* **2016**, *29*, 29–36.

[11] E. Skúlason, V. Tripkovic, M. E. Björketun, S. Gudmundsdóttir, G. Karlberg, J. Rossmeisl, T. Bligaard, H. Jónsson, J. K. Nørskov, *J. Phys. Chem. C* **2010**, *114*, 18182–18197.

Manuscript received: May 22, 2019
Accepted manuscript online: June 12, 2019
Version of record online: July 3, 2019

